Parametric Amplification of Matter Waves in Periodically Translated Optical Lattices

N. Gemelke,[1] E. Sarajlic,[1] Y. Bidel,[1] S. Hong,[1] and S. Chu[1,2]

[1]*Departments of Physics and Applied Physics, Stanford University, Stanford, California 94305, USA*
[2]*Directorate, Lawrence Berkeley National Laboratory, Berkeley, California 94720, USA*

(Received 28 April 2005; published 19 October 2005)

We observe the sudden growth of small classes of Bloch waves from atomic Bose-Einstein condensates held in periodically translated optical lattices. The effect is explained by narrowband parametric amplification of Bloch waves from noise, due to phase-matched scattering of atom pairs out of the condensate. Amplification occurs above a well-defined modulation threshold, described by dynamic shaping of single-particle band structure.

DOI: 10.1103/PhysRevLett.95.170404 PACS numbers: 03.75.Lm, 03.67.−a, 03.75.Be, 03.75.Kk

A major effort since the achievement of Bose-Einstein condensation in neutral atoms has been the development of techniques to generate nonclassical correlations in atomic matter waves [1]. Of particular importance to this goal was the realization that entangled states may be generated by pairwise scattering of atoms out of macroscopically occupied classical states [1–3] into pairs of correlated output modes, in close analogy to optical parametric amplification [4]. Experimental advances along these lines were made with the demonstration of atomic four-wave mixing (FWM) [5,6].

These processes are self-stimulated, resulting in exponential growth of output modes from small seed populations. If the gain is large and restricted to a small number of output modes, a few significantly populated correlated states will grow from broadly distributed noise before the classical source atoms are depleted [6,7]. Gain requires the underlying scattering process be nearly phase matched, conserving both energy and momentum in converting two atoms from source to output states; appropriate control of single-particle dispersion can thereby allow tailored narrowband parametric gain [8].

Recently, use of optical lattices to modify single-particle dispersion has led to dramatic consequences, including localization effects [9,10], gap-soliton formation [11], and modulational instability [12–15]. It was also pointed out that the dispersion introduced by a static lattice might be used to phase match one-dimensional degenerate four-wave mixing [8]. In this Letter, we extend those methods by periodically translating (shaking) an optical lattice, which couples vibrational levels and creates novel band structure. For appropriate modulation parameters, degeneracy is created for Bloch waves near the Brillouin zone center and edge.

Concurrent with this expected degeneracy, we observe instability in a zero-momentum condensate marked by sudden growth of narrow peaks in the momentum distribution at half the lattice recoil momentum, indicating population transfer into band-edge Bloch states (equivalently transient spatial period doubling of the atomic wave function). Instability may be described as the onset of parametric gain due to phase-matched scattering of atoms from the condensate, allowing growth of Bloch waves with a narrow momentum spread from broadly distributed noise. We measure the onset threshold with shaking amplitude and frequency, and show it to be consistent with expected phase-matching conditions, onset of a period-doubling dynamic instability, and numeric evolution of the Gross Pitaevskii Equation (GPE).

To observe the effect, samples of 5×10^4 Bose-condensed ^{87}Rb atoms were prepared in the $|F = 2, m_F = 2\rangle$ hyperfine state with no observable thermal component by evaporative cooling in a triaxial time-orbiting potential trap [16]. After evaporation, the mean magnetic trap frequency was relaxed to $\bar{\omega} = 2\pi \times 37$ Hz, and the condensate was adiabatically loaded over 400 ms into a set of 1, 2, or 3 orthogonal standing waves derived from a 10 W, 1.064 μm Nd:YAG laser. Each standing wave was formed by one retroreflected beam focused to 100 μm at the location of the condensate, intensity stabilized and separated in frequency from the other standing waves by 80 MHz. To shake the lattice, an electro-optic phase modulator was placed in the reflection path of each standing wave. Sinusoidal modulation generated a lattice potential $V(x, t) = V_0 \sin^2[2\pi(x - x_0 \cos\omega_D t)/\lambda]$, where $x_0 = \lambda\phi_0/4\pi$ is the amplitude introduced by phase modulation of depth ϕ_0 at frequency ω_D. The lattice was calibrated by locating the heating resonance corresponding to phase modulation at the lattice vibration frequency ω_v, where $\hbar\omega_v$ is the energy difference between the lowest two band centers. When multiple standing waves were used, intensities were adjusted to equalize their vibration frequencies.

After loading and interrogating condensates in the lattice, the magnetic trap and lattice were switched off in 200 μs, and atoms were absorbtively imaged after 30 ms time of flight. The momentum distribution was inferred from the matter wave interference patterns of the released atoms. Without modulation, we observed interference peaks at momenta $n\hbar\mathbf{k}_0$, where n is an integer and $\mathbf{k}_0$ is an inverse lattice vector, indicating phase-coherent localization in the lattice potential wells. Here, $|\mathbf{k}_0| = 2\pi/a = 4\pi/\lambda$, where a is the lattice spacing. Relative peak heights

were determined by the on-site wave function of the condensate, whose center of mass oscillated when the lattice was shaken near resonance.

Modulating below vibrational resonance in a one-dimensional lattice resulted in growth of narrow peaks at momenta $\pm\hbar k_0/2$ [Fig. 1(a)], which also oscillated in phase with the drive [Fig. 1(b)]. These peaks became visible only beyond a critical frequency-dependent drive amplitude and following sufficient modulation time. For $V_0 = 9E_r$, where $E_r = \frac{\hbar^2 k_0^2}{8m}$ with m the atomic mass, visible onset occurred after a 5 ms modulation pulse with $x_0 > .01a$ at detuning $\delta \equiv \omega_D - \omega_v = -2\pi \times 2$ kHz. The amplitude for critical onset of this momentum class decreased with decreased detuning from resonance (Fig. 2). Following onset, peaks were discernable under drive for 800 cycles (100 ms), before obscured by loss of interference pattern contrast. Similar behavior was observed for $3.9 \leq V_0/E_r \leq 19.5$.

We have investigated dependence of the critical drive parameters on external trapping geometry by varying the envelope trapping frequencies by 30%. This caused no shift in onset amplitude at fixed detuning to 10%. We also observed period doubling in two-dimensional lattices of the same depth with one or both [Fig. 1(c)] axes shaken. Though the interference pattern contrast decreased, no measurable shift in onset amplitude was observed at fixed detuning. In three-dimensional lattices, loss of contrast precluded observation of peaks at $|\mathbf{p}| = \hbar k_0/2$.

Shaking the lattice acts equally on each lattice site and cannot itself induce modulations of the condensate wave function at twice the lattice spacing. Interparticle interaction, however, allows lattice symmetry to be spontaneously broken, permitting coupling to nonzero quasimomentum states. Accordingly, candidate mechanisms for populating the $\pm\hbar k_0/2$ momentum classes likely involve the combined effects of interaction and modulated lattice.

Since the first excited band energy has a comparatively strong, inverted dependence on momentum, small modulation-induced admixtures of these states to the lowest band will dramatically alter single-particle dispersion. Band mixing has previously been described [17] and observed [18] with thermal atoms; its effect becomes more apparent if we consider the two lowest bands in a "dressed" basis set [17]. Here, each basis state is a time-dependent superposition of delocalized ground and excited states with equal quasimomenta q, chosen to make the single-particle Hamiltonian time independent in a rotating wave approximation (RWA), and diagonal. The resulting dressed band structure, $\Lambda_q^{\pm}$ [Figs. 3(a) and 3(b)], may be used to examine stability of stationary states including effects of interaction [19].

We performed linear stability analysis of the lattice-periodicity Bloch states for the lower dressed band Λ_q^- in the tight-binding limit of the GPE, following methods in [12,20]. Adding perturbations of definite momentum to Bloch waves in this band, we identified parameter regions where excitation energies include imaginary values, signaling exponential growth or decay of perturbations. For $\delta < 0$, zero-momentum Bloch states first become dynami-

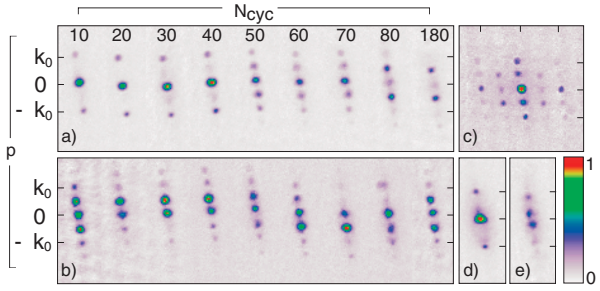

FIG. 1 (color). Absorption images of atomic interference following lattice modulation and time-of-flight expansion. (a) Atoms released at the turning point of lattice translation after a number of cycles $N_{\rm cyc}$. For short modulation times peaks occur only at $p = 0, \pm\hbar k_0$. Subsequently, peaks develop at $p = \pm\hbar k_0/2$. (b) Release occurs in the 76th cycle, spaced by 1/8th of a cycle; center of mass oscillates in phase with applied drive. (c) Simultaneous doubling in 2D lattice applying the same modulation as in (a),(b) to two orthogonal standing waves. (d) Modulation for $\delta > 0$ in 1D lattice; for small amplitudes, the $p = 0$ peak develops a shoulder. At larger amplitudes, (e) broad peaks are apparent between $p = 0$ and $\pm\hbar k_0$. For visibility, (c) shows absorption; (a),(b),(d),(e) show atomic column densities. For (a),(b),(c), $\omega_v = 2\pi \times 10.4$ kHz, $x_0 = .040a$, $\omega_D = 2\pi \times 7.6$ kHz, (d) $\omega_v = 2\pi \times 11.0$ kHz, $x_0 = .035a$, $\omega_D = 2\pi \times 12.5$ kHz. (e) $\omega_v = 2\pi \times 11.0$ kHz, $x_0 = .037a$, $\omega_D = 2\pi \times 12.5$ kHz.

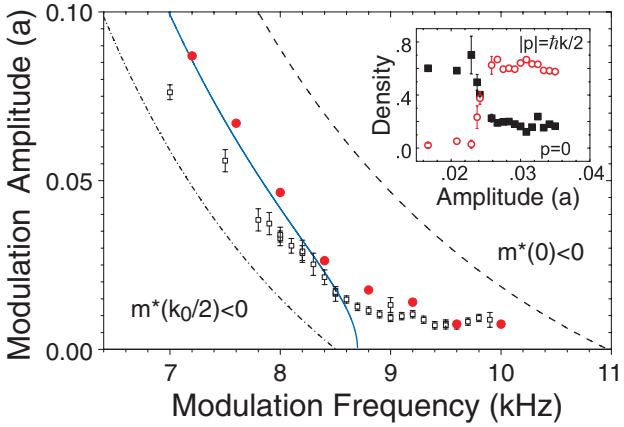

FIG. 2 (color). Measured critical drive strengths and detunings (boxes) and zero-parameter comparison to those predicted by band structure and numeric evolution of the GPE for $\delta < 0$, $\omega_v = 2\pi \times 11.0 \pm 0.1$ kHz. Solid line shows analytic result for equal dressed single-particle energy at lower band center and edge, which occurs for zero drive amplitude at $\delta = J_1 + J_0$. Dashed (dotted) line shows infinite effective mass at band center (edge); between these, mass is positive both at the center and edge. Circles show onset in numeric evolution of the GPE for $J_0 = 0.024E_r$, $J_1 = -0.28E_r$, $U_{00} = U_{10} = (4/3)U_{11} = 2 \times 10^{-4}E_r$; $\omega_{\rm ext} = 2\pi \times 45$ Hz and $N = 5 \times 10^4$. Inset: Relative peak atomic densities at $|p| = 0, \hbar k_0/2$ vs drive amplitude x_0 for $\omega_D = 2\pi \times 8.4$ kHz. Modulation pulse lengths were 10 ms.

cally unstable when the modulation amplitude is increased to equalize single-particle energy at band edge and center [Fig. 3(c)] [21]. This lower threshold is independent of atomic density and interaction strength. Close to onset, exponential growth occurs only for perturbations with momenta near $\pm\hbar k_0/2$ [Fig. 3(d)], consistent with phase-matching criteria and experimental observations. This is in contrast with observations of broadband modulational instability [13–15]. The predicted threshold amplitudes are smaller than necessary to invert effective mass at band center, and show quantitative agreement with data (Fig. 2) for large negative detunings. This interpretation fails for small detuning, where interaction energy exceeds the dressed band gap, introducing non-negligible level mixing.

The calculations in Fig. 2 use knowledge only of the measured ω_v, from which we calculate unperturbed band structure, tunneling amplitudes J_σ for each band σ, and Wannier wave functions $\phi_\sigma(x)$. Coupling between bands is modeled by converting to a frame moving with the lattice [17], resulting in a single-particle Hamiltonian $H_{\rm sp} = p^2/(2m) + V(x,0) - m\omega_D^2 x x_0 \cos\omega_D t$. Lattice modulation is then replaced by inertial force, yielding an interband coupling strength $\hbar\Omega = m\omega_D^2 x_0 \int dx \phi_0^* x \phi_1$; for stability analysis, intraband effects of inertial force are neglected. On-site interaction energy is estimated by approximating the wave function transverse to the lattice $\psi(\mathbf{r}_\perp)$ by a Thomas-Fermi profile corresponding to measured transverse trapping frequencies and average occupation number γ. On-site interaction energy between atoms in bands σ and σ' is given by $U_{\sigma\sigma'} = (2 - \delta_{\sigma\sigma'})U_0 \int d\mathbf{r} |\Phi_\sigma|^2 |\Phi_{\sigma'}|^2$, where $\Phi_\sigma(\mathbf{r}) = \psi(\mathbf{r}_\perp)\phi_\sigma(x)$, $U_0 = 4\pi\hbar^2 a_s/m$, and a_s is the s-wave scattering length. We take $U_{\sigma\sigma'}$ independent of site and occupation number; more accurate treatments may be found in [22,23].

To model dynamics and provide analysis independent of the dressed band interpretation, we numerically evolved the GPE in the tight-binding limit for two coupled (bare) bands of the shaken lattice. Using approaches from [24,25], the condensate wave function was described by a complex site-dependent amplitude $c_{j,\sigma}$ for each (bare) vibrational level σ. The wave function $\Psi(\mathbf{r}) = \sum_j c_{j,\sigma} \times \Phi_\sigma(\mathbf{r} - j\mathbf{a})$ was substituted into the time-dependent GPE, and the $c_{j,\sigma}$ were numerically evolved according to

$$
\begin{aligned}
i\hbar\dot{c}_{j,\sigma} = & -J_\sigma(c_{j+1,\sigma} + c_{j-1,\sigma}) + V_j^\sigma c_{j,\sigma} + \frac{U_{\sigma\sigma}}{2}|c_{j,\sigma}|^2 c_{j,\sigma} \\
& + \frac{U_{\sigma\sigma'}}{4} c_{j,\sigma'}^2 c_{j,\sigma}^* + \frac{U_{\sigma\sigma'}}{2}|c_{j,\sigma'}|^2 c_{j,\sigma} \\
& + \hbar\Omega\cos(\omega_D t) c_{j,\sigma'}, \qquad (1)
\end{aligned}
$$

where

$$
\begin{aligned}
V_j^\sigma = & \hbar\omega_v \delta_{1,\sigma} - m\omega_D^2 x_0 \cos(\omega_D t) ja \\
& + \frac{m\omega_{\rm ext}^2}{2}(ja - x_0\cos\omega_D t)^2 \qquad (2)
\end{aligned}
$$

represents the band energy, intraband effect of inertial force, and external trapping potential, respectively. The

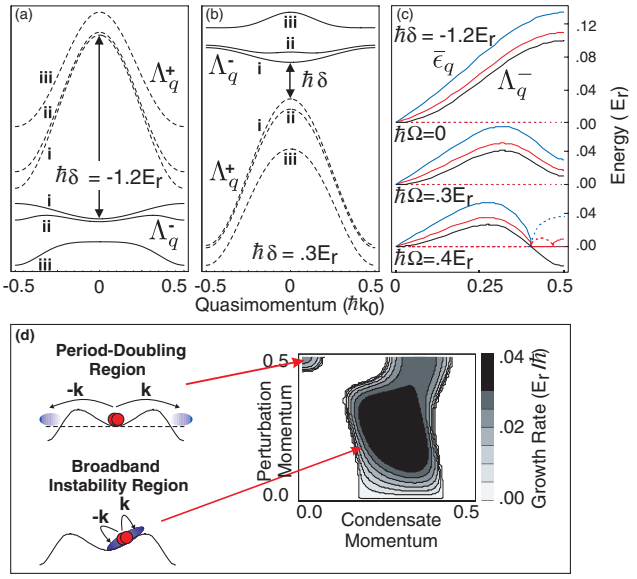

FIG. 3 (color). Renormalized band structure for $\delta < 0$ (a) and $\delta > 0$ (b), obtained by diagonalizing the single-particle Hamiltonian in the RWA for the two lowest bands. Solid (dashed) lines indicate energy $\Lambda_q^-(\Lambda_q^+)$ of the renormalized ground (excited) band, for coupling strengths $\hbar\Omega/E_r$ of (i) 0, (ii) 0.3, and (iii) 0.9. (c) Lowest band single-particle Λ_q^- and elementary excitation $\bar{\epsilon}_q$ energy for three drive strengths. Solid (dashed) line shows real (imaginary) part of $\bar{\epsilon}_q$ for $\gamma U_{00} = 0.005E_r$ (red) and $0.02E_r$ (blue). Lattice depth is $V_0 = 10.5E_r$. (d) Growth rates in dynamically unstable regions as function of condensate and perturbation momenta, from linear stability analysis of the GPE in the lower dressed band; $\hbar\delta = -1.2E_r$ $\hbar\Omega = 0.35E_r$, $\gamma U_{00} = 0.02E_r$.

calculation was initialized with a wave function confined to the lowest band, solved to be stationary without modulation, and normalized according to the experimental atom number. The calculation was performed with external potential comparable to the experiment, and number of sites chosen to safely exceed the number occupied.

The parameters for onset of population at $\pm\hbar k_0/2$ for negative drive detunings show good agreement with the experiment (Fig. 2), and agree with predictions for instability at the center of the lower dressed band described above. No instability was observed in the same numeric evolution for an excited band with positive tunneling amplitude.

To investigate the role of external trapping potential, we compared period-doubling onsets with and without $\omega_{\rm ext}$. To reduce numeric artifacts from the large inertial force and boundary effects, this comparison was done in the stationary frame, to first order in x_0. Without $\omega_{\rm ext}$, periodic boundary conditions were used with a site number (40) comparable to the experiment. In this case, a small seed population at $p = \pm\hbar k_0/2$ grew rapidly above the threshold modulation strength. Without seed population, observable peaks at $\pm\hbar k_0/2$ did not occur for experimentally relevant time scales. For $\omega_{\rm ext} = 2\pi \times 45$ Hz, seed popu-

lation was guaranteed by the finite extent of the condensate, and resulted in observable population at $p = \pm\hbar k_0/2$ after modulation times comparable to those in the experiment.

Experimentally, seeds may arise from other sources, notably thermal population and localization. Unfortunately, imaging sensitivity prohibited direct measurement of initial population at $p = \pm\hbar k_0/2$. Future study may use Bragg scattering or localization in deep lattices [9] to introduce seed to measure gain and growth rate.

It is instructive to consider the microscopic description of the period-doubling instability. In the standard Bogoliubov theory of elementary excitations of a condensate, the Hamiltonian for noncondensed particles (created by $a_k^\dagger$) is [1]

$$\mathcal{H} = \sum_{k\neq 0} (\epsilon_k + n_0 U_0) a_k^\dagger a_k + \frac{1}{2} n_0 U_0 (a_k^\dagger a_{-k}^\dagger + a_k a_{-k}), \quad (3)$$

or $\mathcal{H} \equiv \sum_{k\neq 0} \bar{\epsilon}_k \alpha_k^\dagger \alpha_k$, where the energy of a quasiparticle of momentum $\hbar k$ (created by $\alpha_k^\dagger$) is $\bar{\epsilon}_k = \sqrt{(\epsilon_k + n_0 U_0)^2 - (n_0 U_0)^2}$. Here, ϵ_k is the single-particle dispersion ($\epsilon_{k=0} \equiv 0$), and n_0 is the condensate density. For an isolated lower dressed band in the tight-binding limit of the shaken lattice, we may take $\epsilon_k = \Lambda_k^- - \Lambda_0^-$ and $n_0 U_0 \approx \gamma U_{00}$. Instability occurs for $-2\gamma U_{00} \lesssim (\Lambda_k^- - \Lambda_0^-) < 0$ [Fig. 3(c)], in agreement with the GPE analysis described above.

Choosing modulation parameters such that $\Lambda_k^- - \Lambda_0^- = -\gamma U_{00}$, the energetic cost for scattering a pair of atoms with opposite momenta from the condensate [demanded by the first term of (3)] is eliminated, resulting in a Hamiltonian for the mode k of $\mathcal{H}_k = \gamma U_{00}(a_k^\dagger a_{-k}^\dagger + a_{-k} a_k)$. This is equivalent to the well-known result for quantum mechanical parametric oscillation [4]. As previously described [2–4,6], $\mathcal{H}_k$ is capable of generating nonclassical correlation in the output modes $\pm k$. The process may be interpreted as degenerate four-wave mixing [8], where the condensed mode simultaneously plays the role of two input waves mixing with output waves of momenta $\pm\hbar k$. In neither free space nor the lowest band of a static lattice can this process conserve energy for a condensate at rest, due to the monotonic increase of single-particle energy ϵ_k with momentum $\hbar|k|$. In a shaken lattice, energy is conserved by including the transfer of energy contained in the coherent vibration of input and output waves in the lattice. In experiments demonstrating nondegenerate four-wave mixing in free space [6], signal gain was limited by unnecessary amplification of many noise-seeded modes. The shaken lattice offers advantage by restricting modes with gain to one dimension [8], *and* to a small range of momenta near the band edge by carefully controlling modulation [Figs. 3(c) and 3(d)]. Gain might be achieved at other momenta by adding weak coupling to higher bands in the lattice.

The analyses above apply for modulation below resonance, where influence of the avoided crossing in Fig. 3 is strongest at the band edge. Experimentally, modulation above resonance results in the appearance of a shoulder around the $p = 0$ peak, followed by growth of broad peaks around $p = \pm\hbar k_0/2$ [Figs. 1(d) and 1(e)] as drive amplitude is increased. While this might be expected from the band structure of Fig. 3(b)(ii), the behavior is not fully understood.

In conclusion, we have observed instability of a ^{87}Rb condensate held in a shaken optical lattice potential. Simple phase-matching arguments qualitatively agree with measured threshold modulation parameters, while stability analysis and numeric evolution of the GPE quantitatively agree. These descriptions are consistent with instability caused by phase-matched parametric gain due to pairwise scattering of atoms from the condensate. This is to our knowledge the first observation related to dynamic band shaping for Bose-condensed atoms in an optical lattice, and its first use to produce controlled, narrowband phase matching in a one-dimensional nonlinear atom-optical process.

We wish to thank M. Kasevich, A. Tuchman, S. Harris, C. Pethick, Congjun Wu, and S. Zhang for helpful discussions. This work was supported in part by Grants from AFOSR and the NSF (phy-0400866-001).

[1] P. Meystre, *Atom Optics* (AIP/ Springer, New York, 2001), and references therein.
[2] H. Pu and P. Meystre, Phys. Rev. Lett. **85**, 3987 (2000).
[3] L. M. Duan *et al.*, Phys. Rev. Lett. **85**, 3991 (2000).
[4] W. H. Louisell, A. E. Siegman, and A. Yariv, Phys. Rev. **124**, 1646 (1961).
[5] L. Deng *et al.*, Nature (London) **398**, 218 (1999).
[6] J. M. Vogels, K. Xu, and W. Ketterle, Phys. Rev. Lett. **89**, 020401 (2002).
[7] V. A. Yurovsky, Phys. Rev. A **65**, 033605 (2002).
[8] K. M. Hilligsoe and K. Molmer, Phys. Rev. A **71**, 041602(R) (2005).
[9] M. Greiner *et al.*, Nature (London) **415**, 39 (2002).
[10] C. Orzel *et al.*, Science **291**, 2386 (2001).
[11] B. Eiermann *et al.*, Phys. Rev. Lett. **92**, 230401 (2004).
[12] B. Wu and Q. Niu, Phys. Rev. A **64**, 061603(R) (2001).
[13] F. S. Cataliotti *et al.*, New J. Phys. **5**, 71 (2003).
[14] L. Fallani *et al.*, Phys. Rev. Lett. **93**, 140406 (2004).
[15] M. Cristiani *et al.*, Opt. Express **12**, 4 (2004).
[16] W. Petrich *et al.*, Phys. Rev. Lett. **74**, 3352 (1995).
[17] R. Diener and Q. Niu, J. Opt. B **2**, 618 (2000).
[18] K. W. Madison *et al.*, Phys. Rev. Lett. **81**, 5093 (1998).
[19] Alternative methods might be provided by Tozzo *et al.*, cond-mat/0505625.
[20] M. Machholm *et al.*, Phys. Rev. A **69**, 043604 (2004).
[21] N. Gemelke *et al.* (to be published).
[22] A. Smerzi and A. Trombettoni, Phys. Rev. A **68**, 023613 (2003).
[23] L. Salasnich, A. Parola, and L. Reatto, Phys. Rev. A **65**, 043614 (2002).
[24] A. Trombettoni and A. Smerzi, Phys. Rev. Lett. **86**, 2353 (2001).
[25] G. L. Alfimov *et al.*, Phys. Rev. E **66**, 046608 (2002).